Geophys. J. Int. (2003) **155,** 857–869

Shear-induced pressure changes and seepage phenomena in a deforming porous layer – I

N. Petford and M. A. Koenders

Centre for Earth and Environmental Science Research, Kingston University, Surrey KT1 2EE, *UK. E-mail: N.Pet@kingston.ac.uk*

Accepted 2003 July 1. Received 2003 June 30; in original form 2002 November 15

SUMMARY

We present a model for flow and seepage in a deforming, shear-dilatant sensitive porous layer that enables estimates of the excess pore fluid pressures and flow rates in both the melt and solid phase to be captured simultaneously as a function of stress rate. Calculations are relevant to crystallizing magma in the solidosity range 0.5–0.8 (50–20 per cent melt), corresponding to a dense region within the solidification front of a crystallizing magma chamber. Composition is expressed only through the viscosity of the fluid phase, making the model generally applicable to a wide range of magma types. A natural scaling emerges that allows results to be presented in non-dimensional form. We show that all length-scales can be expressed as fractions of the layer height H, timescales as fractions of $H^2(n\beta'\theta + 1)/(\theta k)$ and pressures as fractions of $R\dot{c}_0 H^2/(\theta k)$. Taking as an example the permeability k in the mush of the order of magnitude 10^{-15} m^2 Pa^{-1} s^{-1}, a layer thickness of tens of metres and a mush strength (θ) in the range 10^8–10^{12} Pa, an estimate of the consolidation time for near-incompressible fluids is of the order of 10^5–10^9 s. Using mush permeability as a proxy, we show that the greatest maximum excess pore pressures develop consistently in rhyolitic (high-viscosity) magmas at high rates of shear ($\dot{c}_0 > 10^{-1}$ Pa s^{-1}), implying that during deformation, the mechanical behaviour of basaltic and rhyolitic magmas will differ. Transport parameters of the granular framework including tortuosity and the ratio of grain size to layer thickness (a/H) will also exert a strong effect on the mechanical behaviour of the layer at a given rate of strain. For dilatant materials under shear, flow of melt into the granular layer is implied. Reduction in excess pore pressure sucks melt into the solidification front at a velocity proportional to the strain rate. For tectonic rates (generally 10^{-14} s^{-1}), melt upwelling (or downwelling, if the layer is on the floor of the chamber) is of the order of cm yr^{-1}. At higher rates of loading comparable with emplacement of some magmatic intrusions ($\sim 10^{-10}$ s^{-1}), melt velocities may exceed effects due to instabilities resulting from local changes in density and composition. Such a flow carries particulates with it, and we speculate that these may become trapped in the granular layer depending on their sizes. If on further solidification the segregated grain size distribution of the particulates is frozen in the granular layer, structure formation including layering and grading may result. Finally, as the process settles down to a steady state, the pressure does not continue to decrease. We find no evidence for critical rheological thresholds, and the process is stable until so much shear has been applied that the granular medium fails, but there is no hydraulic failure.

Key words: dilatancy, filtration, granular flow, melt, porous media, shear.

1 INTRODUCTION

The processes governing the solidification of chambered magma have received considerable attention over the last two decades, and much progress has been made in understanding the thermal and physical behaviour in both the fluid-dominated regime (e.g. Huppert *et al.* 1984; Turner & Campbell 1986; Jupart & Tait 1995; Jellinek & Kerr 1999) and the process of solidication (Marsh 1988; Martin 1990; Worster *et al.* 1990; Marsh 1996; Hort *et al.* 1999). Studies of the freezing process have shown that for a considerable part of the crystallization interval, the material can be treated effectively as a saturated porous medium. Movement of pore fluid due to instabilities caused by buoyancy effects in multiphase flows has been investigated both numerically (e.g. Drew 1971; McKenzie 1984; Scott & Stevenson 1986; Sleep 1988; Spiegelman *et al.* 2001) and experimentally (Kerr & Tait 1986; Tait & Jaupart 1992; Renner

et al. 2000). Spiegelman (1993) has investigated the flow of melt in a strain-rate sensitive, deformable porous medium for a forced melt flux driven by buoyancy. However, the mechanical effects of externally induced shearing on the porous matrix, and its subsequent rheological behaviour are less well studied, despite abundant field and petrological evidence showing that many igneous materials, irrespective of composition and tectonic setting, have undergone significant amounts of shearing, whilst still in a partially molten state (e.g. Nicolas 1986; Brown & Rushmer 1997). This paper is intended to remedy that situation to some extent. It deals with a theoretical exploration of the deformation and associated fluid flow processes that occur during a shearing strain path imposed on a strain sensitive porous layer in the presence of a confining stress. The changes in the solid volume fraction that take place during the process are especially important to acquire insight into the fluid flow pattern that results. The idea is put forward that the system, so modelled, has many of the mechanical properties of a porous crystal mush in a magma chamber, and that the effects that are calculated using the model can be identified with measured position-dependent grain size distribution and crystal content. Thus, by measuring the latter the model predictions can be verified to some extent.

The primary objective of the analysis is to explore what set of conditions leads to a stable situation. An analysis that enables the distinction between processes that settle down into stability and ones that eventually display runaway behaviour is required. The latter set of problems would obviously lead to either an ongoing change in the material properties until a more-or-less constant state is achieved, or result in some catastrophic set of events that would lead to an entirely different conformation of material properties.

This work expands upon an earlier quantitative treatment by Koenders & Petford (2000), for a simple geometry with idealized material properties, which provides analytical solutions for the macroscopic behaviour of magma under pure shearing motion. The theory employed builds on the work by Biot (1941), extending it from the strict isotropic material that this author envisaged, to include more general deformation features such as dilatant effects. A key finding that will be reproduced below is the fact that a steady state (if it exists) occurs after a transient set of changes. It is found that the characteristic time required for the steady state to become manifest is, generally speaking, fortuitously short when compared with a characteristic geological timescale, earthquake loading being the exception. As the theory does not deal with dynamic processes anyway, it is possible to consider slow behaviour only. Where no steady state results, the initial stage is investigated to obtain the most likely location of material failure. One of the key extensions of the analysis over previous work is that compressible fluids are considered, rather than incompressible ones. Also, much more complicated geometries are investigated. In addition it is shown that the mechanical responses of the mixture under shear may have a bearing on some long-standing problems in igneous petrology such as the development of flow fabrics, grain size distribution and sorting and layering in magmatic rocks.

The material properties of granular materials are summarized first; then a mathematical analysis is carried out, leaving the technical details to an Appendix. Two distinct geometries are investigated. The first, a 1-D calculation of the deformation and magma flow in a two-layer model, is similar to that considered by Koenders & Petford (2000) for deformation in a crystallizing magma mush. The second, to be addressed in a companion paper (Koenders & Petford in preparation, 2003), consists of a three-layer problem, where the middle layer is deformable and shear-sensitive. Whilst the geometry investigated is limited to a 1-D calculation, the essence of a number of geophysically relevant situations is captured in this way, thus achieving new insight into the rheological behaviour of the solid matrix and associated pressure changes in the melt-phase during deformation.

2 GRANULAR MATERIALS

The magmatic mush material is assumed to be granular in nature (e.g. Mead 1925). This would follow from a heterogeneous crystallization process, and differs from the semi-empirical approach used by Paterson (1995) to model granular flow of partially molten rock by plastic deformation and pressure melting of grains. The stiffness of the grains in this material is assumed to be large compared with both the ambient pressure and stress changes that occur in the period after crystallization. Under these conditions a deviatoric load—notably in the context here, a simple shearing strain path—gives rise to an *expansive* volume change. This effect is commonly referred to as dilatancy; it is observed in tests on dry granular materials under low stress (typically the ratio of the Young's modulus of the grains to the isotropic stress is greater than 100); the soil mechanics literature may be consulted: Lambe & Whitman (1979) and see also for example Arthur & Phillips (1975). Despite its common occurrence, there is some debate as to what exactly causes this effect. It is important to distinguish between pre-failure and post-failure behaviour. Pre-failure the material is elastic or elasto-plastic, though not necessarily isotropic. Post-failure the material has become degenerate, though not unconstrained. The transition between the two regimes is marked by some form of bifurcation, see for instance Molenkamp (1985) or Vermeer (1990) for continuum-mechanical descriptions in the context of elasto-plasticity.

The dilatant effect is almost unique to granular materials (stiff clays also exhibit it to some extent). It is therefore not unexpected that workers in the field of granular mechanics have tried to attribute it to a particulate mechanism. Reynolds (1885) hypothethized a mechanism in which grains 'ride up' against one another. This feature is very easy to visualize, but requires that the grain motion organizes itself in slip bands. The latter are a post-bifurcation phenomenon.

The link between particulate motion and a continuum description, which accounts for large groups of grains, is still not entirely resolved to a satisfactory conclusion. The so-called 'double-shearing model' that describes the post-bifurcation regime has been put forward by Spencer (1964) and de Josselin de Jong (1977). The slip bands cut through the material causing it to be structured in parallellomorphic blocks; their direction is given by the maximum obliquity direction as dictated by Coulomb's friction criterion (see Arthur & Dunstan 1982). Dilatancy arises from roughness on the surfaces of the blocks, caused by the particulate nature of the material, see Koenders (1990) for the details for the mathematics of this model.

Pre-failure descriptions of dilatancy cannot be associated with slip bands. Rowe (1962) puts forward a two-particle model, the motion of which is (descriptively) embedded in the continuum motion of the granular assembly. In a recent paper by Goddard & Didwania (1998) this concept is further explored in the light of quasi-static numerical simulations of granular assemblies. Using Cundall's numerical simulation (Cundall & Strack 1982), Kuhn (1999) has demonstrated that certain modes of granular material deformation can still be regarded as being 'organized'. Gaspar & Koenders (2001a) have shown that such organization is the result of naturally occurring

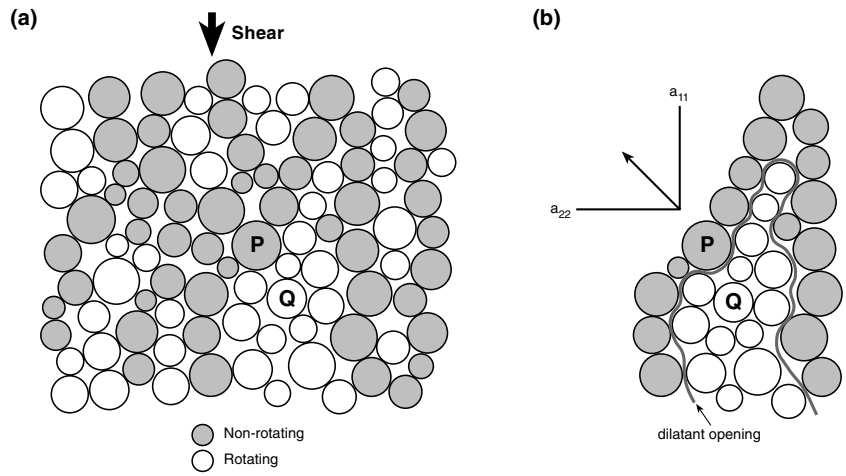

Figure 1. Schematic representation of dilatant behaviour in a permeable layer during shear based on the numerical simulations of Stefanovska (1996). (a). P and Q represent two connected rigid domains made up of assemblages of rotating and non-rotating (spectator) grains. (b). Shear-induced slip between adjacent rigid domains results in dilatant opening.

heterogeneity in a granular material. It would therefore be likely that dilatancy is to a large extent associated with sensitivity of deformation to the natural non-homogeneity of the material. This sensitivity is exacerbated as the load is persistently deviatoric. Detailed investigation of numerical simulation data has shown that many of the overall continuum stiffness components can be understood in this way: Gaspar & Koenders (2001b) and Gaspar (2002). A feature of pre-failure deformation that emerges from both Kuhn and Gaspar & Koenders' approaches to the subject is the relevance of processes that take place on a scale that is much smaller than the overall aggregate size, but substantially larger than the two-grain size accounted for by the earlier description by Rowe. The existence of the 'meso-scale' is further illustrated in an approach by Stefanovska (1996), using a least-squares quasi-static simulation method (Koenders & Stefanovska 1993). While Kuhn and Gaspar & Koenders looked for deformation features, Stefanovska sought to characterize the medium in terms of connected slip domains. She succeeded in identifying such domains in pre-peak conditions at higher stress ratios (see Fig. 1.)

Linear elastic isotropic modelling of the material as envisaged by Biot (1941), will not give rise to a volume change under shear. Therefore, a somewhat extended model is introduced that can accommodate volume changes under shear loading. Such a model is incremental and intrinsically anisotropic. Thus the stress rate and the deformation rate are related by a general incremental stiffness tensor, which is called $\boldsymbol{a}$ and has the dimensions of a stress.

The incremental moduli are not constants during a stress path, but depend on the state of the assembly, its microscopic (mineral) properties and the state of evolution it is in. Rapid changes in the moduli are observed in the vicinity of the critical density (when the material changes over from contracting to dilatant behaviour), but outside this point the changes are relatively minor with increasing stress ratio. This finding inspires an approach in which the moduli can be regarded as being more or less constant, representing asymptotic branches of the behaviour. Thus, if pure shear is the only component of the skeletal stress that evolves and the problem is independent of the horizontal coordinate x, one may write the stress–strain incremental behaviour in terms of the instantaneous moduli $\boldsymbol{a}$, linking the velocity gradients (rate of strain tensor) to the skeletal shear stress rate,

$$\dot{\sigma}'_{12} = \frac{1}{2} a_{1212} \frac{\partial \dot{u}}{\partial y} + a_{1222} \frac{\partial \dot{v}}{\partial y} \tag{1}$$

$$\dot{\sigma}'_{21} = \frac{1}{2} a_{2112} \frac{\partial \dot{u}}{\partial y} + a_{2122} \frac{\partial \dot{v}}{\partial y}. \tag{2}$$

Here, u and v are the horizontal and vertical displacements and the skeletal stress is denoted by $\boldsymbol{\sigma}'$, where compressive stresses are negative, in line with the usual continuum mechanics description (see Becker & Burger 1975). The rate of change is indicated by the time derivative 'flux dot'. The rate of volume change is $\partial \dot{v}/\partial y$. Both stress and strain are symmetric tensors and therefore eqs (1) and (2) are identical: $a_{1222} = a_{2122}$ and $a_{1212} = a_{2112}$. For expanding, dilating materials in pure shear $\partial \dot{v}/\partial y$ is positive and the parameter a_{2212} has the opposite sign to the shear stress rate; for contracting materials a_{2212} has the same sign as the shear stress rate. The reader is referred to the Appendix for further expansion. A list of values and parameters used in the calculations are given in Table 1.

All the above pertains to dry material, with the skeletal stress being the stress that results from grain contact interaction in the granular matrix. Application to fluid-saturated media requires an extension of the stress definition to allow for pore pressures so that the material behaviour, as captured in the stress–strain relationship, can be connected to porous media flow phenomena. The mathematical model developed here is based on the equations of linear poroelasticity proposed by Biot (1941), modified to take into account the effects of shear-induced dilatancy in granular materials by coupling the volumetric strain to the deviatoric (shearing) stress (Koenders 1997; Koenders & Petford 2000). Biot's theory is relevant to deforming magma as it contains a number of terms that describe important physical variables of the system, including melt viscosity, permeability, as well as the moduli of the granular framework.

The effect of dilatancy is that pore space becomes available for the pore fluid. In a crystallizing magma, the petrological implications are that as pore space opens up, the reduced pressure draws fresh melt from below up into the solidification front. This idea is in itself not new, for example Emmons (1940) recognized that dilatant rifting of a dense crustal mush would draw melt into the voids, a process referred to by Carmichael *et al.* (1974) as autointrusion. A conceptual appreciation of this effect is key to understanding

Table 1. Units and variables.

Symbol	Parameter	Value/unit
a	Grain size	m
$\boldsymbol{a}$	Stiffness tensor	Pa
$\dot{c}_0$	Shear stress rate	Pa s^{-1}
G	Principal modulus	10^9 Pa
H	Layer depth	m
k	Permeability	m^2 Pa^{-1} s^{-1}
n	Porosity	0.2–0.5
p	Excess pore pressure	Pa
t	Time	s
u	Horizontal displacement	m
v	Vertical displacement	m
y	Position	m
$\dot{e}$	Strain rate	s^{-1}
β'	Fluid compressibility	Pa^{-1}
η	Melt viscosity	Pa s
ϕ_s	Solidosity (crystal load)	0.5–0.8
$\Delta\rho$	Density contrast	kg m^{-3}
θ	Stiffness of mush	10^9 Pa
$\boldsymbol{\sigma}'$	Skeletal stress (matrix)	Pa
γ	Tortuosity	1
R	Moduli ratio	1

our analysis of both the two- and three-layer problems. Despite its apparent simplicity, it has been a non-trivial task to capture this behaviour mathematically and to obtain an exact analytical solution to Biot's equations that include dilatancy (see the Appendix). This approach does not include temperature effects, though these can be added later as a refinement. The other effect which is not captured in the description is the effect of creep in the skeleton. This effect would give the granular matrix (anisotropic) viscous properties as well as stiffness properties. Spiegelman (1993), in contrast, considers purely viscous effects and no stiffness of the matrix, while more recently the role of viscoelastic matrix behaviour in deformable porous media has been assessed (e.g. Connolly & Podladchikov 1998; Vasilyev *et al.* 1998). In the analysis here it is assumed that time-dependent effects are dominated by the fluid flow viscosity, relegating constitutive creep to a second-order analysis, which—like thermal phenomena—may be added as a refinement to the analysis afterwards.

Biot's equations (see Biot 1941), express the continuity of the fluid, compressible phase in a granular environment, assuming Darcyan porous medium flow with position-dependent permeability $k(\mathbf{x})$. The permeability here is scaled to the unit weight of the fluid, and its dimension (m^2 Pa^{-1} s^{-1}) is thus that of a (superficial) velocity $v_s = -k\nabla p$. (Note that this definition differs from many geological applications where the permeability is scaled to the viscosity of the fluid.) Biot's equation is now made special to the 1-D approximate geometry to hand. If the porosity of the medium is n and the fluid compressibility is β' it reads as

$$\frac{\partial}{\partial y}\left[k(y)\frac{\partial p}{\partial y}\right] = n\beta'\frac{\partial p}{\partial t} + \frac{\partial \dot{v}}{\partial y}, \tag{3}$$

where p is the excess pore pressure, defined as the difference between the fluid pressure minus the hydrostatic pressure. Eq. (3) is solved in two geometries, the first is a one-layer system modelling the mushy zone in which crystallization has taken place to a sufficient degree that the crystal content (solidosity, ϕ_s) is in the range $0.5 < \phi_s < 0.8$, and overlaps with the upper limit of the critical rheological melt fraction ($0.7 < \phi_s < 0.8$) of Arzi (1978) and proposed percolation thresholds of Vigneresse *et al.* (1996). The second is a three-layer geometry, which has sufficient unique features of its own to warrant a separate paper.

3 ONE-LAYER SYSTEM

In order to formalize our model in a geological context, we have adopted the terminology of Marsh (1996) used to define the structure of a solidification front in a crystallizing magma. The rheological divisions in a solidification front are shown schematically in Fig. 2, and serve as a useful reference frame from which to construct a physical model of crystallizing magma under externally imposed deformation. Shearing of the solidification front may result from either tectonic motions during crystallization, syn-emplacement deformation or deformation associated with chamber expansion due to fresh inputs of magma. Note that according to the Marsh classification, our investigation is confined mostly to a layer within the rigid crust of the solidification front ($\phi_s > 0.55$). As shown below, although a region of relatively high strength, it can easily dilate during shear. Influx of any melt upwards into the rigid crust is likely to have an important modifying effect on its rheology (see the discussion section).

The geometry of the one-layer system is shown in Fig. 2. The top is defined as $y = 0$ and the bottom as $y = -H$. In modelling it is assumed that the top of the region is virtually impermeable, implying that the pressure gradient vanishes: $\partial p/\partial y(0) = 0$. The bottom is regarded as being entirely fluid, so that the permeability is infinite and all components of the incremental stiffness tensor for the solid framework $\boldsymbol{a}$ vanish. Only pure shearing stress external loading is envisaged and this load increases with time from $t = 0$ at a rate of $\dot{c}_0$.

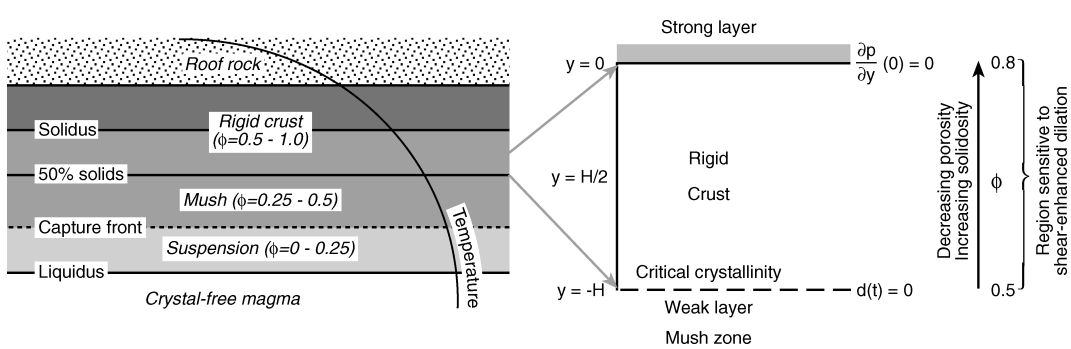

Figure 2. Rheological divisions within a crystallizing magma (after Marsh 1996), and the position and geometry of the modelled deforming layer. The layer has a depth of $y = -H$, and a solidosity (ϕ_s) interval of 0.5–0.8 (porosity of 50–20 per cent). Its mass loading exceeds the critical crystallinity of $\phi_s = 55$ per cent and corresponds to the rigid crust portion of the solidification front.

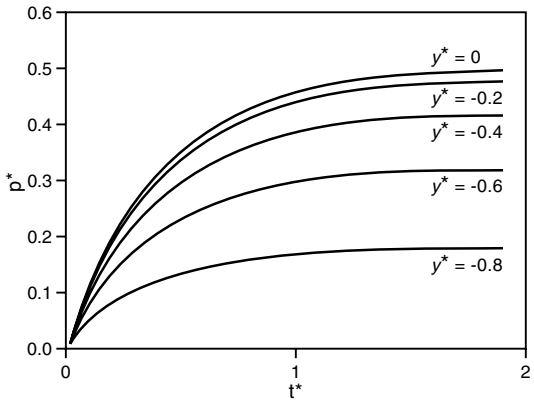

Figure 3. The scaled pressure ($p*$) in the deforming layer as a function of the scaled time (t^*) and position (y^*). Note the maximum excess pressure occurs at position $y^* = 0$, and becomes asymptotic at $t^* > 1$.

In order to model this system the main approximation is that the material parameters can be regarded as constants throughout the region of interest, as well as over the whole period of time. Two convenient stiffness related parameters are the mean values of $\theta \equiv (a_{1212}a_{2222} - a_{2212}a_{1222})/a_{1212}$ and a parameter $R \equiv a_{2212}/[a_{1212}(n\beta'\theta + 1)]$.

An important result of the analysis is that the solution for this system can be expressed entirely in non-dimensional parameters. All length-scales can be expressed as fractions of H, all timescales as fractions of $H^2(n\beta'\theta + 1)/(\theta k)$ and all pressures as fractions of $R\dot{c}_0 H^2/(\theta k)$. The solution of the excess pore pressure as a function of the position and time is depicted in terms of these non-dimensional parameters in Fig. 3. It is observed that the scaled time it takes the pressure to reach its end-value is of the order of $t^* = 1.5$ or $t = 1.5H^2(n\beta'\theta + 1)/(\theta k)$. It is of practical interest to estimate a value for the consolidation time of the problem. Taking as an example the permeability in the mush being $\sim 10^{-15}$ m^2 Pa^{-1} s^{-1}, the layer thickness of the order of magnitude of tens of metres and the value of θ in the range 10^8–10^{12} Pa, leads to an estimate of the consolidation time for near-incompressible fluids of the order of 10^5–10^9 s. For all types of loading relevant to geological processes, bar earthquake loading (Koenders & Petford 2000), this represents a short timescale. Thus, the pressure distribution that is appropriate to slow geological processes is the end-of-process parabolic profile, derived in the Appendix,

$$p(y, \infty) = R\dot{c}_0 \frac{H^2 - y^2}{2k\theta}. \tag{4}$$

For dilatant materials under shear, a flow from the bottom into the granular layer is implied. A further note is that the process settles down to a steady state; the pressure does not continue to decrease. The process is stable until so much shear has been applied that the granular medium fails, but there is no hydraulic failure.

4 RESULTS

Some of the geological applications of the one-layer model have already been described elsewhere (Koenders & Petford 2000; Petford & Koenders 2001). An essential feature of the model with regard to the deformation of solidification fronts in crystallizing magma chambers is the introduction of two temporally variable (but coupled) stress terms, one for the solid matrix and an independent fluid (melt) pressure. Both can be assessed as a function of increasing strain rate to see under what conditions the mush is likely to fail, and to gain an impression of the magnitude of fluid upwelling that accompanies dilation in the solid granular matrix. While the analysis does not include the effects of temperature explicitly, it does allow magma composition to be expressed through the viscosity of the melt, thus allowing an assessment of the effect of shear-induced dilatancy in both mafic and felsic systems at crystal loads >50 per cent.

For our analysis we make the distinction between three different loading regimes: (1) background lithospheric or plate tectonic strain rates ($\sim 10^{-14}$ s^{-1}); (2) emplacement loading ($\sim 10^{-10}$ s^{-1}), based on estimates from field studies in and around granitic intrusions and silicic lava domes (Fernandez & Castro 1999; Castro *et al.* 2002); and (3) earthquake loading (10^{-3} s^{-1}) as an example of extreme quasi-static loading. Meaningful comparisons between different magma compositions and solid matrix depend on the order of magnitude of the various parameters that appear in the theory. The parameter R essentially gives the ratio between moduli, modified by the compressibility of the fluid; this parameter is of the order of unity—positive when the material is contractive and negative in the dilatant regime. The order of magnitude of the parameter θ is that of the principal stiffness components of the mush; this quantity follows from measurements and is of the order of 10^8–10^9 Pa. The permeability k is estimated from a non-dimensional tortuosity parameter γ, the mean grain size a and the fluid viscosity η and has the form $k = \gamma a^2 n^3/\eta$. Finally, the loading parameter $\dot{c}_0$ is estimated from the loading strain rate $\dot{e}$ and the mean value of the principal shear modulus G: $\dot{c}_0 = G\dot{e}$. The main sensitivity of the problem thus follows from an estimate of the mean value of the pressure $\overline{p}$, the order of magnitude of which is evaluated according to expression (4). This estimate leads to a rough value of all the stress changes in the system. What it does not tell us is how the skeletal stress ratio evolves; this quantity gives information on the point at which failure in the mush will take place. At failure (and beyond), no sensible calculation can be made, as mathematically the system becomes critically sensitive to the boundary conditions, changing as it does from the quasi-static elliptical regime to the hyperbolic or parabolic regime. From a constitutive point of view, the situation at failure also changes: the effects of creep and localization can no longer be considered to be small.

Using the above estimates for the various variables, the mean pressure has the order of magnitude of $R\dot{e}\eta(H/a)^2/\gamma$. Both R and γ are non-dimensional and therefore the product $\dot{e}\eta$ represents a quantity with the dimension of a pressure.

4.1 Stress changes in the granular matrix

The total stress in the vertical direction remains constant and therefore the accumulated vertical skeletal stress equals the generated pore pressure. Now, it is clear from the previous sections that the latter attains a constant value after a period of time that is long compared with $H^2(n\beta'\theta + 1)/(\theta k)$. Using the estimates from the previous section this characteristic time is of the order of $(H/a)^2\eta/G$. For geological purposes this is a very short time (10^4 s for granitic magmas, for example). The ratio of the time constant to the shear strain rate then gives some impression as to whether the consideration of only the final state is justified. It is seen that for all loading types, except the fast earthquake loading, the ratio of the time constant to the shear strain rate is much less than unity.

The picture that emerges, therefore, is that the excess pore pressure—and with it the accumulated normal vertical stress—settles down to a fixed, position-dependent value. Meanwhile the

shear stress is continually increased. The deviatoric skeletal stress therefore increases all the time, while the isotropic stress remains fixed at a value. Failure phenomena for materials such as these mushes that are under low isotropic stress (low, that is, compared with their mineral stiffness) are controlled by the stress ratio. After a period of time these mushes 'fail'; this is the bifurcation phenomenon described earlier. When this point is crossed the mechanical response of the system becomes critically dependent on the boundary conditions, though the constraints that still exist in the system prescribe certain preferential directions along which localized shear planes can form. The geological manifestation of such failure would be the melt-filled shear zones commonly observed in migmatites and other anatectic rocks (e.g. Brown & Rushmer 1997).

An order of magnitude estimate of the isotropic skeletal stress follows from the consideration that the grains are buoyant and a first-order estimate follows from the stress associated with the buoyancy. If the mass density difference is called $\Delta\rho$, the mean position in the thickness of the crystallized layer is $H/2$; therefore the mean isotropic stress equals $\Delta\rho Hg/2$. Typically this is $\sim 10^4$ Pa. The stress ratio to failure is of the order of 0.2–0.5, depending on a large number of factors: pre-stress, roughness, porosity are all factors that play a role. For a shear rate $\dot{e}$ and mean shear stiffness G, an estimate of the time when deviatoric stress and isotropic reach the failure criterion ratio is of the order of $\Delta\rho Hg/(2G\dot{e})$. In practical cases this value is still a factor of some 100–10 000 times greater than the time constant of the system.

For a system like this, in which the normal stresses are quite small compared with the mineral stiffness values, brittle failure (particle crushing) is obviously not relevant. Such a mechanism is more likely in systems in which the isotropic stress increases due to an increase in the extraneous load; the three-layer model under development (Koenders & Petford 2003) is an example.

4.2 Excess pore fluid pressure

We are now in a position to make a number of statements regarding the change in pore fluid pressure during shear that apply to both basaltic and rhyolitic crusts. Figs 4 and 5 show the range in excess pore fluid pressure (Pa) as a function of layer position for an applied strain rate ($\dot{e}$) of 10^{-14} and 10^{-10} s^{-1} calculated using eq. (4). Individual curves relate to melt fractions (n) of 0.2–0.5. Layer composition was simulated using the interstitial melt viscosity (η) as a proxy, with values of 10^2 and 10^5 Pa s equating to a hypothetical basalt (Fig. 4) and a rhyolite layer (Fig. 5), respectively. A grain size effect is also included. As expected, the maximum excess pore pressure occurs at position $y = 0$. At a given strain rate and mean grain size, the effect of decreasing the mush porosity results in progressively higher excess pore fluid pressures. Against this, an increase in the mean layer grain size results in an order of magnitude drop in excess pressure. This effect is shown clearly in both Figs 4 and 5, where at a constant (tectonic) loading rate of 10^{-14} s^{-1}, an increase in grain size from 1 to 5 mm lowers the maximum pore pressure from $\sim 10^{-3}$ to 10^{-4} Pa (basalt, Figs 4a and b) and 6 to 0.25 Pa (rhyolite, Figs 5a and b). These changes can be understood by considering the effects of changing porosity (melt fraction) and grain size on the transport properties of the layer. The effect of reducing both is to lower the permeability, resulting in correspondingly higher excess pore pressures at a given rate of shear and fixed melt viscosity.

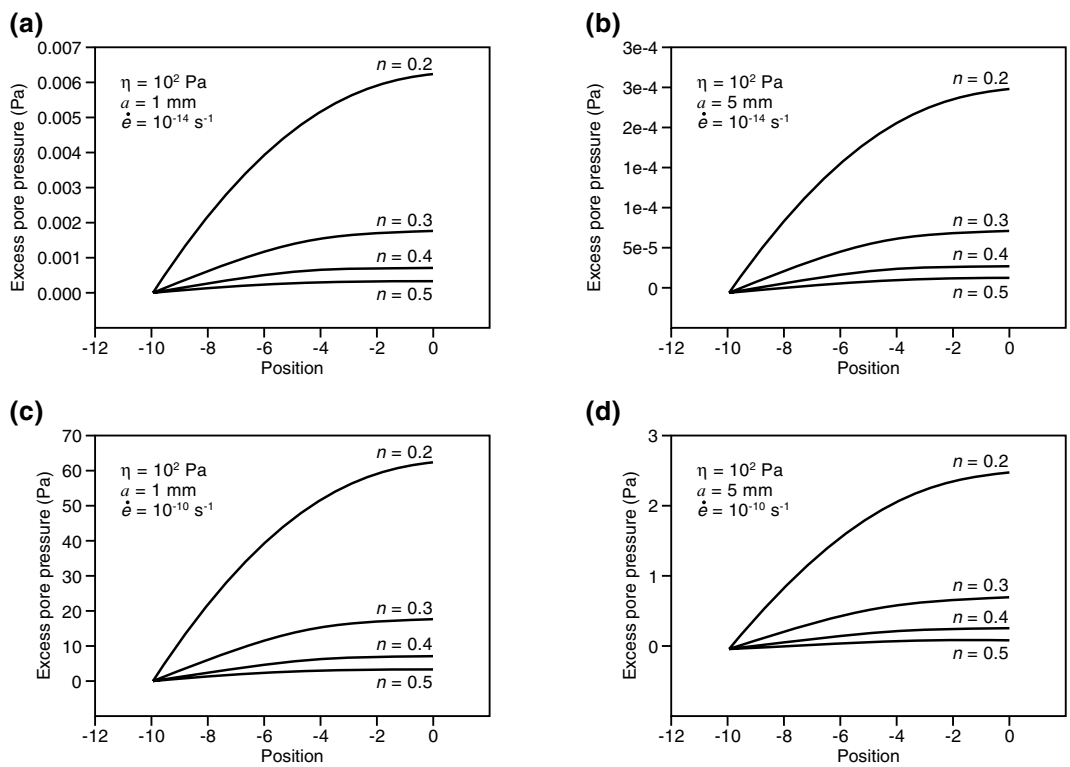

Figure 4. (a)–(d) Increase in excess pore fluid pressure (Pa) in a porous layer of basaltic composition (interstitial melt viscosity $=10^2$ Pa s) as a function of shear stress rate and grain size (a). Individual curves show the pressure range for a fixed melt fraction (porosity, n) over the range 0.2–0.5. Strain rates of 10^{-14} s^{-1} (a) and (b) and 10^{-10} s^{-1} (c) and (d) relate to average plate tectonic and pluton emplacement loading conditions, respectively. Layer permeability (k) ranges from 8×10^{-11} m^2 Pa^{-1} s^{-1} ($a = 1$ mm, $n = 0.2$) to 3×10^{-8} m^2 Pa^{-1} s^{-1} ($a = 5$ mm, $n = 0.5$). The greatest excess pressures occur in layers with lowest permeabilities at high strain rates (Fig. 4c).

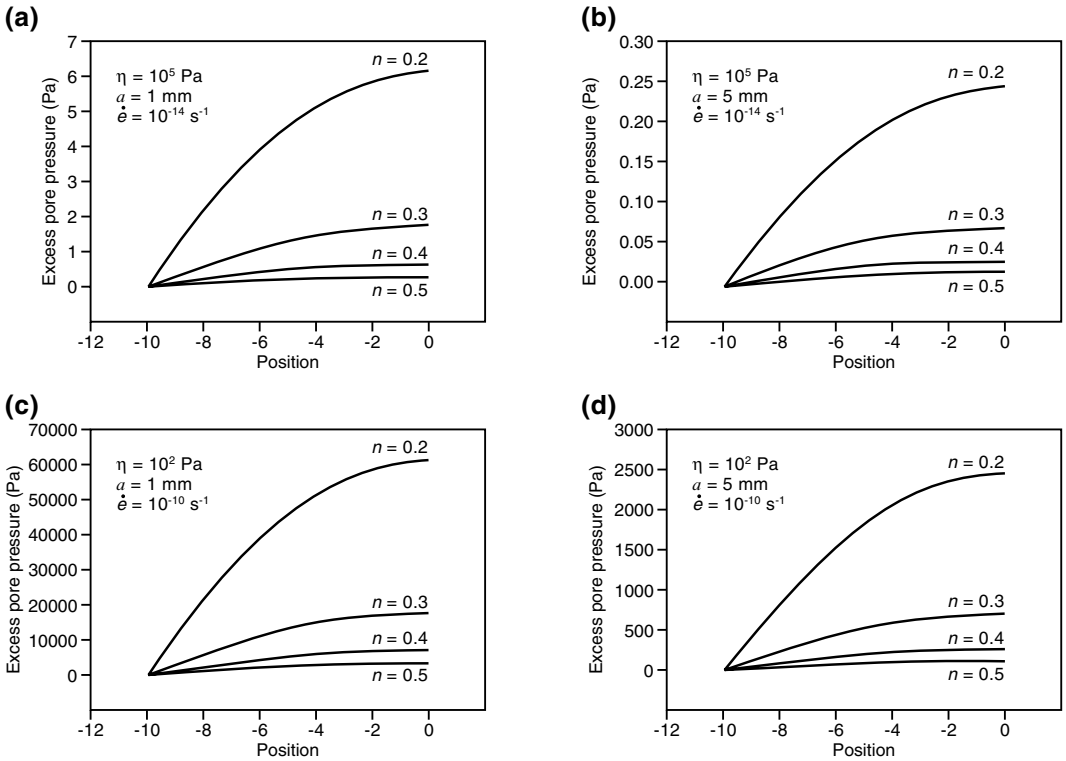

Figure 5. (a)–(d) Increase in excess pore fluid pressure (Pa) in a porous layer of rhyolite composition (interstitial melt viscosity $=10^5$ Pa s) as a function of shear stress rate and grain size (a). Individual curves and strain rates labelled as in Fig. 4. Layer permeability ranges from 8×10^{-14} m^2 Pa^{-1} s^{-1} ($a = 1$ mm, $n = 0.2$) to 3×10^{-11} m^2 Pa^{-1} s^{-1} ($a = 5$ mm, $n = 0.5$). Maximum excess pore pressures are $>10^4$ Pa (Fig. 5c).

Higher excess pore pressures are induced at higher shear stress rates. Thus, deforming a layer at loading rates comparable with magma emplacement (10^{-10} s^{-1}), produces a much stronger effect that either reduction in grain size or porosity. The greatest maximum excess pore pressures occur where high shear stress rates are combined with the smallest layer permeabilities (Figs 4c and 5c). Thus, for a basalt system with a grain size of 1 mm and porosity of 20 per cent ($k = 8 \times 10^{-10}$ m^2 Pa^{-1} s^{-1}), the calculated excess pressure is 63 Pa. For more viscous rhyolites, this value is $\sim 6 \times 10^4$ Pa (Fig. 5c). These values fall to $\sim$2.5 and 2500 Pa, respectively, when the grain size is increased to 5 mm (Figs 4d and 5d).

Comparison of Figs 4 and 5 indicate that the melt viscosity exerts a strong influence on the likely range of excess pore pressures during shear, with greatest excess pressures occurring in deformable layers with the most viscous interstitial liquids. This effect is explored further in Fig. 6, where the maximum excess pore pressure is plotted as a function of melt fraction for three fluid viscosities of 10^1, 10^3 and 10^5 Pa s corresponding to typical basalt, andesite and rhyolite melts (e.g. McBirney 1984), for two loading rates of 10^{-14} and 10^{-10} s^{-1}. At tectonic strain rates, maximum excess pressures are $\ll$1 Pa for permeabilities corresponding to basaltic mushes, reaching a maximum value of $\sim$10 Pa in rhyolites. However, at rates typical of emplacement loading, an increase of $O(10^4)$ in excess pressure is predicted, with maximum values for rhyolitic permeabilities approaching 10^5 Pa (1 bar, Fig. 6c). Similar excess pressures will only occur in fine-grained basaltic crusts where the porosity is of the order of a few per cent. While shear-induced values of excess pore fluid pressure for most magma types should fall within a permeability range of $\sim 10^{-9}$–10^{-14} m^2 Pa^{-1} s^{-1}, we note in passing that it is possible to calculate excess pressures at much higher strain rates. Thus, for quasi-instantaneous (earthquake) loading at a shear stress rate of 10^6Pa s^{-1}($\dot{e} = 10^{-3}$ s^{-1}), the porous layer is predicted to develop excess pressures in the range 10–100 MPa. However, the validity of the dilatancy theory is limited to the range in which the constituent grains are much stiffer than the isotropic stress, greater than 1 per cent, say. The former quantity is estimated to be some 10^7–10^8 Pa and therefore at these high stresses, grain deformability may take place and the theory would need refinement in this loading regime.

5 DISCUSSION

5.1 Melt upwelling rates

The excess pressures developed in the solid matrix described above are accompanied by a simultaneous reduction in excess pore pressure that sucks melt into the solidification front at a rate proportional to the shear rate. At tectonic strain rates, melt upwelling velocities are small and of the order of mm yr^{-1}. However, at higher rates more typical of emplacement, laminar upwelling velocities can reach 3 m yr^{-1} (Table 2). As the problem is phrased in terms of shear strain rates, then the melt upwelling velocity is independent of viscosity. This is because the dilatant matrix volume change rate operates as a constraint and therefore the volume rate of flow is entirely defined by the constraint. It is noted that this is a matter of phaseology: had the problem been defined in terms of shear stress rates, then the permeability properties *would* have been important for the flow rates (and the strain rates would follow from the analysis).

These higher rates exceed those predicted due to melt instability in undeformed rhyolitic systems of 10^{-7}–10^{-1} m yr^{-1} (Barboza &

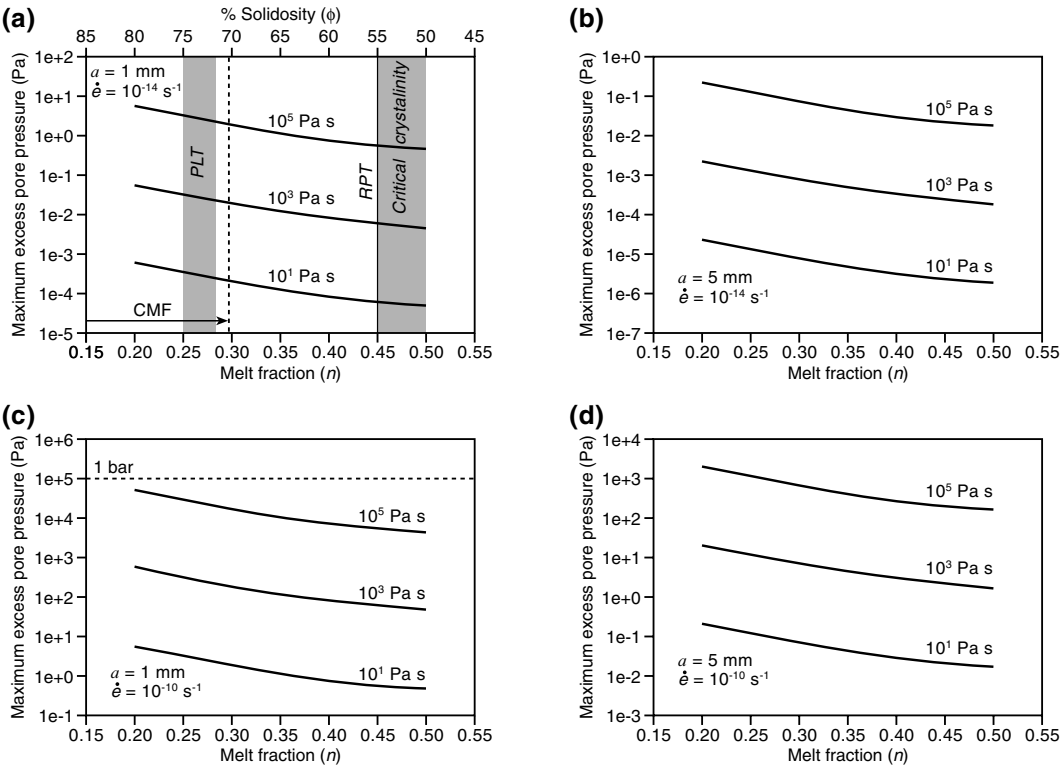

Figure 6. (a)–(d) Plots showing maximum excess pore pressure as a function of melt fraction for three melt viscosities in the range $10^1 > \eta > 10^5$ Pa s, equating to basalt, andesite and rhyolite liquors. The maximum excess pore pressure is strongly dependent on both shear stress rate and melt viscosity, with highest values predicted in the most evolved (viscous) magmas. The ruled lines in Fig. 6(a) correspond to proposed rheological thresholds in crystallizing silicic magmas (after Vigneresse *et al.* 1996), at 55 per cent solids (rigid percolation threshold) and 72–75 per cent solids (particle locking threshold). CMF is the critical melt fraction (after Wickham 1987). The generic critical crystallinity at between 50–55 per cent solids is from Marsh (1981).

Table 2. Melt flow rates in the porous magmatic layer described in the text as a function of strain rate.

Loading regime	Strain rate	Melt flow rate
Tectonic	10^{-14} s^{-1}	10^{-11}–10^{-12} m s^{-1}
Emplacement	10^{-10} s^{-1}	10^{-7}–10^{-8} m s^{-1}
Earthquake	10^{3} s^{-1}	1–0.1 m s^{-1}

Bergantz 1998) and are comparable with melt upwelling velocities beneath Mid Ocean Ridges (e.g. Kelemen *et al.* 1997). For the extreme case of near instantaneous shear arising from earthquakes, flow rates of up to 1 m s^{-1} are predicted while the quake is active. By implication, shear-induced flow may be locally important in transporting heat and chemical components from the mainly fluid region beneath the capture front, into the solidification zone itself. This raises the possibility that some types of chemical zonation and resorbtion seen commonly in crystals (especially plagioclase) in plutonic rocks and their volcanic equivalents are due not to large-scale magma chamber processes such as influx of mafic magma and chamber-wide circulation of individual phenocrysts (e.g. Knesel *et al.* 1999), but a much more subtle effect due to local flow of melt into the expanding pore space of the crystal mush and crust.

5.2 Rheological thresholds

As shown previously (Figs 4–6), the strong influence of melt viscosity on excess pressure implies that the rheological behaviour of basaltic and rhyolitic magmas during shear will differ. The role of suspended solids in controlling the flow behaviour of magmas has attracted considerable attention, and a number rheologically identifiable zones in magmas have been defined, most famously the rheological critical melt percentage (RCMP) or the critical melt fraction (CMF) of Arzi (1978) and Van der Molen & Paterson (1979). The CMF has classically been used to describe a transition in granitic magmas from a viscous fluid at low crystal contents ($\lesssim$40 per cent) to an 'elastic solid' at melt fractions $\lesssim$0.3, where movement is resisted primarily by a skeletal matrix of touching grains (e.g. Wickham 1987). Most recently, this inequality has been revised downwards to melt fraction in the range 0.03–0.08 (Rosenberg & Handy 2003). Although the experiments on which the concept rests has been challenged (Rutter & Neumann 1995), such transitions are used commonly to speculate on the physical state of the magma during emplacement-related deformation (e.g. Paterson *et al.* 1998). Vigneresse *et al.* (1996) proposed that during crystallization, magmas will encounter a percolation threshold at 55 per cent solids (corresponding with the upper limit of critical crystallinity of Marsh), and another at 72–75 per cent solids. However, a major source of uncertainty in these qualitative models is that while capable of providing descriptive accounts, they are unable to explain the fundamental macroscopic behaviour of the melt–crystal mixture as it deforms. The transition from rate-dependent to elasto-plastic behaviour is known to depend upon the applied strain rate (e.g. Dell'Angelo & Tullis 1988). This prompts the question whether the viscous behaviour of the pore fluid plays a role in the (shear) stress controlled deformation process (Renner *et al.* 2000). As we have shown here and elsewhere (Koenders & Petford 2000; Petford 2003), the interplay between the deformation of the granular framework and the

flow of the pore fluid is time-dependent, meaning that the positioning of rheological thresholds is at best arbitrary, the one exception being the critical crystallinity (Marsh 1981). A proper treatment requires the solution of the relevant differential equations (see the Appendix). The parameter estimates outlined here describing the various stress changes in the solid matrix, along with permeability features, open up a robust way of understanding the mechanical response of crystallizing magma during deformation. Consideration of Fig. 6 for example, shows that while the change in melt fraction encompasses the rheological thresholds set out above, there is no evidence for bifurcation or sudden jumps in excess pore pressures that might be interpreted as critical. Furthermore, it challenges the assertion of Vigneresse & Tikoff (1999) that above 75 per cent solids, the system is locked to any further melt flow. Recent work on load-bearing granular materials has shown that while the close packing of particles can result in jamming and rigidity, they cannot become permanently jammed, and that sudden changes in applied stress can produce non-equilibrium transitions from solid to fluid-like states (Cates *et al.* 1998). Such media are referred to as fragile, and although a constant volume effect (no dilatancy is implied), we speculate that some rigid magmas undergoing shear may behave in an analogous fashion. Where this leaves current rheological models for granitic magmas is uncertain, and more detailed experimental and theoretical work is needed in order to confirm the existence of the proposed rheological thresholds.

5.3 Filtration and flow of crystals

A further consequence of deformation-induced melt upwelling is that non-buoyant crystals of a certain size dilutely mixed in the magma may be kept in suspension that might otherwise sink due to gravity. Assuming no yield strength in the melt, it is possible from Stokes law to make a first-order approximation of the typical grain size (radius) that can be kept afloat within the solidification front as a function of strain rate. This is shown in Fig. 7, where at tectonic strain rates only very small grains (radius 0.01–0.04 mm) that are negatively buoyant with respect to the parent melt will be prevented from sinking. However, emplacement loading will produce upflow sufficient to suspend grains with diameters of up to ∼1 cm. For the extreme case of earthquake loading, flow rates may become briefly non-laminar and able to support blocks up to 20 m in diameter.

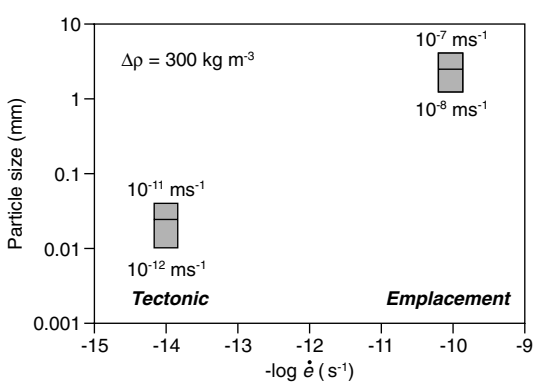

Figure 7. Plot of particle size versus strain rate, showing the approximate range in particle size that could be kept afloat in a dilute mixture of non-buoyant crystals by upwelling melt beneath the sheared layer. Higher strains in the granular matrix result in higher mean flow rates, so that for strain rates accompanying pluton emplacement, grains in excess of 1 mm can be kept in suspension that might otherwise sink under gravity (calculated using Stokes law with a density contrast between grain and melt of 300 kg m^{-3}).

Upwelling melt may also carry particles with it that depending upon their size, become captured in the granular layer inside the solidification front (see Marsh 1988), reducing its permeability. This processes, in which a porous layer (or filter) becomes clogged by finer particles is well known to geotechnical engineers and leads to a reduction in hydraulic conductivity (Brauns *et al.* 1993). A similar clogging process may explain some of small- to medium-scale heterogeneity common in many granitic rock textures (Petford 1993), and is worthy of further investigation. Crystals with high aspect ratios, such as alkali and plagioclase feldspar pheoncrysts, may also be susceptible to rotation and alignment in the direction of flow. Some possible consequences of shear-induced melt upwelling into the deforming layer are summarized in Fig. 8. We speculate that on further solidification, any flow segregated grain size distribution or crystal alignments may become frozen in, offering an explanation for the graded layering found in some plutonic rocks (e.g. Barriére 1981), not easily explained by simple gravity settling.

5.4 Limits of the model

It is well known that at the high temperatures accompanying magma solidification, thermally induced crystal plasticity is likely to play an important role in governing the medium-term rheological behaviour of the mixture (e.g. Kohlstedt & Zimmerman 1996). While our model does not explicitly account for creep, thermally activated processes are likely to govern the rheological behaviour of partially molten rocks at strain rates of $\sim 10^{-10}$ s^{-1} where the confining pressure is also high (Stevenson 1989). Thus, our constant value for the stiffness of the mush ($\theta = 10^9$ Pa) is unlikely to remain fixed during any prolonged period of deformation for loading in excess of plate tectonic rates. Other factors contributing to the mush permeability including melt viscosity, melt fraction (porosity) and tortuosity will also play an important role in governing the overall mechanical behaviour of the system. None will remain constant as crystallization proceeds, and while a full sensitivity analysis of the relative importance of each variable in time is required to isolate the key effects, it is likely that simple grain size variations will play a dominant role. For example, an increase in mean grain size, and the depth of the crystallizing layer H, will reduce the excess pore fluid pressure at a given strain rate due to the strong dependence of permeability on the matrix transport properties (e.g. Dullien 1992). It could be argued that by examining strictly mechanical processes only, no real insight is attained, as any instability may also follow from non-mechanical changes. Nevertheless, we consider it exceedingly useful to have the mechanical part understood, as this gives the first link between the geometry of the problem and the pressures that arise. Also, the mechanics serves as an outer envelope in the parameter space for the separation of stable from unstable regions. A further shrinking of the stable region due to any non-mechanical processes can be undertaken at a later stage. Naturally, if one is interested in coming to some form of classification of catastrophes, a more extended analysis is required.

6 CONCLUSIONS

We have presented a quantitative description of the mechanical behaviour of a porous layer ($n = 0.2$–0.5) in a shear field using a modified form of Biot's theory of poroelasticity. Equations appropriate to the geometry are derived, and predictions of the pressure

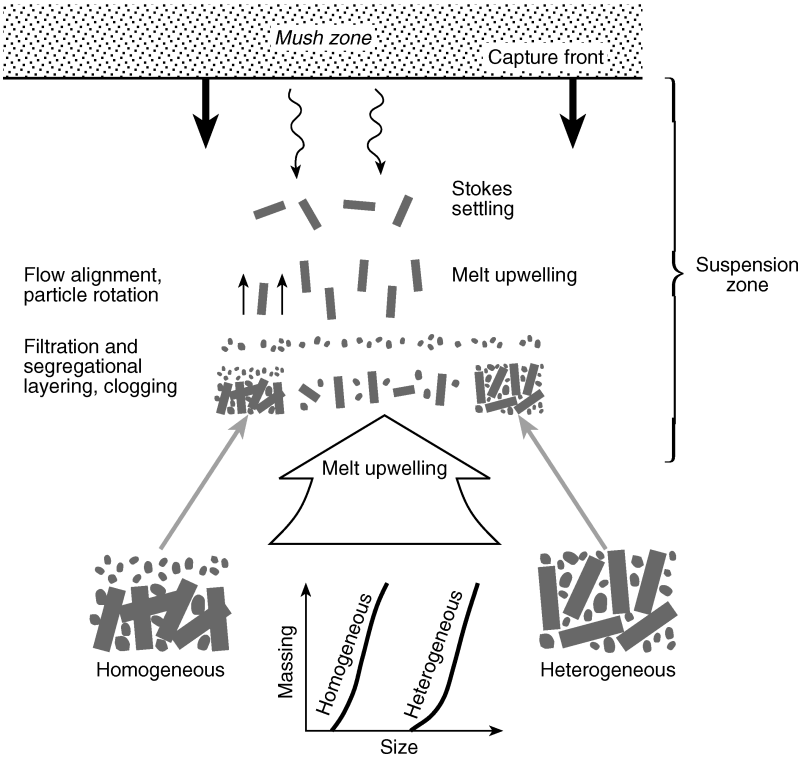

Figure 8. Schematic depiction of shear-induced upwelling of melt into the mush zone from beneath the capture zone (Marsh 1988, 1996), highlighting some possible grain size distributions and orientations resulting from shear-induced melt flow. Filtration effects including layering (Koenders & Kilchherr 2002), clogging and flow alignment of early formed pheoncrysts or entrained solids are implied. Possible end-member particle size distributions for homogenous and heterogeneous filters and particle gradation band curves, based on filtration models for soils (Brauns *et al.* 1993) are shown.

changes and rate of melt flow in the porous crystal framework as a function of strain rate are made for a range of geological loading conditions. The mechanical response of the mixture to shear scales with the melt viscosity, the mean particle size and the square of the layer depth. The results, in dimensionless form, are applicable to a number of geophysically relevant situations where magma of varying composition is undergoing externally imposed deformation. Our initial results suggest that mafic and felsic magmas with crystal contents in the range 50–80 per cent will respond differently to shearing, with felsic systems being much more likely to develop high excess pore fluid pressures. Local flow rates, induced by pressure changes in the crystal matrix due to dilatancy are strain rate dependent and increase with increasing stress rate. Shear-induced flow may promote both particle alignment and filtration effects, thus providing an explanation for some types of layering due to variations in grain size observed in plutonic rocks.

ACKNOWLEDGMENTS

We would like to thank two anonymous reviewers who helped to improve the clarity of the manuscript.

REFERENCES

Arthur, J.R.F. & Dunstan, T., 1982. Rupture layers in granular media, in *Deformation and Failure of Granular Materials,* pp. 453–460, eds Vermeer, P.A. & Luger, H.J., Balkema, Rotterdam.

Arthur, J.R.F. & Phillips, A.B., 1975. Homogeneous and layered sand in triaxial compression, *Gèotechnique,* **25,** 799–815.

Arzi, A.A., 1978. Critical phenomena in the rheology of partially melted rocks, *Tectonophysics,* **44,** 173–184.

Barboza, S.A. & Bergantz, G.W., 1998. Rheological transitions and the progress of melting crustal rocks, *Earth. planet. Sci. Lett.,* **158,** 19–29.

Barriére, M., 1981. On curved laminae, graded layers, convection currents and dynamic crystal sorting in the Ploumanac'h (Brittany) subalkaline granite, *Contribs. Min. Pet.,* **77,** 214–224.

Becker, E. & Burger, W., 1975. *Kontiuumsmechanik,* p. 228, Teubner, Stuttgart.

Biot, M.A., 1941. General theory of three dimensional consolidation, *J. Appl. Phys.,* **12,** 155–164.

Brauns, J., Heibaum, M. & Schuler, U., eds, 1993. *Filters in Geotechnical and Hydraulic Engineering,* Balkema, Rotterdam.

Brown, M. & Rushmer, T., 1997. The role of deformation in the movement of granitic melt: views from the laboratory and the field, in *Deformation-Enhanced Fluid Transport in the Earth's Crust and Mantle,* Vol. 8, pp. 111–144, ed. Holness, M.B., *Min. Soc.* London series.

Carmichael, I.S.E., Francis, J.T. & Verhoogen, J., 1974. *Igneous Petrology,* p. 739, McGraw-Hill, New York.

Castro, J, Manga, M. & Cashman, K., 2002. Dynamics of obsidian flows inferred from microstructures: insights from microlite preferred orientations, *Earth planet. Sci. Lett.,* **119,** 211–226.

Cates, M.E., Wittmer, J.P., Bouchauad, J.-P. & Claudin, P., 1998. Jamming, force chains and fragile matter, *Phys. Rev.,* **81,** 1841–1844.

Connolly, J.A.D. & Podladchikov, Yu.Yu., 1998. Compaction-driven fluid flow in viscoelastic rock, *Geodynamica Acta,* **11,** 55–84.

Cundall, P.A. & Strack, O.D.L., 1982. A discrete numerical model for granular assemblies, *Géotechnique,* **29** (1), 47–65.

de Josselin de Jong, G., 1977. Mathematical elaboration of the double sliding, free rotating model, *Arch. Mech.,* **29,** 561–591.

Dell'Angelo, L.N. & Tullis, J., 1988. Experimental deformation of partially melted granitic aggregates, *J. Metamorphic. Geol.,* **6,** 495–615.

Drew, D., 1971. Average field equations for two-phase media, *Stud. Appl. Maths,* **50,** 133–166.

Dullien, F.L.A., 1992. *Porous Media Fluid Transport and Pore Structure,* Academic, New York.

Emmons, R.C., 1940. The contribution of differential pressures to magmatic differentiation., *Am. J. Sci.,* **238,** 1–21.

Fernandez, C. & Castro, A., 1999. Pluton accommodation at high strain rates in the upper continental crust. The example of the Central Extremadura batholith, Spain, *J. Struct. Geol.,* **21,** 1143–1149.

Gaspar, N., 2002. Structures and heterogeneity in deforming, densely packed granular materials, *PhD thesis,* Kingston University.

Gaspar, N. & Koenders, M.A., 2001a. Micromechanic formulation of macroscopic structures in a granular medium, *J. Eng. Mech. (ASCE),* **127,** 987–993.

Gaspar, N. & Koenders, M.A., 2001b. Estimates of the shear modulus of a granular assembly using heterogeneous media techniques, *Proc. Powders and Grains*, May 21–25, 2001, Sendai, Japan, pp. 165–168, A. A. Balkema Publishers, Rotterdam.

Goddard, J.D. & Didwania, A.K., 1998. Computations of dilatancy and yield surfaces for assemblies of rigid frictional spheres, *J. Mech. Appl. Math.,* **51,** 15–43.

Hort, M., Marsh, B.D., Resmini, R.G. & Smith, M.K., 1999. Convection and crystallisation in a liquid cooled from above: an experimental and theoretical study, *J. Petrol.,* **40,** 1271–1300.

Huppert, H.E., Sparks, R.S.J. & Turner, J.S., 1984. Some effects of viscosity on the dynamics of replenished magma chambers, *J. geophys. Res.,* **89,** 6857–6877.

Jellinek, A.M. & Kerr, R.C., 1999. Mixing and compositional stratification procuced by natural convection 2. Applications to the differentiation of basaltic and silicic magma chambers and komatiite lava flows, *J. geophys. Res.,* **104,** 7203–7218.

Jupart, C. & Tait, S., 1995. Dynamics of differentiation in magma reservoirs, *J. geophys. Res.,* **100,** 17 615–17 636.

Kelemen, P.B., Hirth, G., Shimizu, N., Speigelman, M. & Dick, H.J.B., 1997. A review of melt migration processes in the adiabatically upwelling mantle beneath oceanic spreading ridges, *Phil. Trans. R. Soc. Lond.*, A, **355,** 283–318.

Kerr, R.C. & Tait, S.R., 1986. Crystallisation and compositional convection in a porous medium with application to layered igneous intrusions, *J. geophys. Res.,* **91,** 3591–3608.

Knesel, K.M., Davidson, J.P. & Duffield, W.A., 1999. Evolution of silicic magma through assimilation and subsequent recharge: evidence from Sr isotopes in sanidine phenocrysts, Taylor Creek rhyolite, NM., *J. Petrol.,* **40,** 773–786.

Koenders, M.A., 1990. Localised deformation using higher order deformation gradients, *J. Energy Res. Technol. (Trans. ASME),* **112,** 51–53.

Koenders, M.A., 1997. A model of a granular assembly as a structured material, *Proc. ASCE Symp. on Mechanics of Deformation and Flow of Particulate Materials,* pp. 11–23, eds Misra, A., Chang, C.S., Liang, R.Y. & Babic, M., American Soc. of Civil Engineers, New York.

Koenders, M.A. & Kilchherr, R., 2002. Structure formation of slurries in heterogeneous porous media, *J. Phys. D,* **35,** 1–8.

Koenders, M.A. & Petford, N., 2000. Quantitative analysis and scaling of sheared granitic magmas, *Geophys. Res. Lett.,* **27,** 1231–1234.

Koenders, M.A. & Petford, N., 2003. Flow and seepage pheonomena in a deforming porous layer: 2, in preparation.

Koenders, M.A. & Stefanovska, E., 1993. The numerical simulation of a dense assembly of particles with elasto-frictional interaction, *Powder Tech.,* **77,** 115–122.

Kohlstedt, D.L. & Zimmerman, M.E., 1996. Rheology of partially molten mantle rocks, *Ann. Rev. Earth planet. Sci.,* **24,** 41–62.

Kuhn, M., 1999. Structured deformation in granular materials, *Mech. Mater.,* **31,** 407–429.

Lambe, T.W. & Whitman, R.V., 1979. *Soil Mechanics,* SI version, *Series in Soil Engineering*, Wiley, New York.

McBirney, A.R., 1984. *Igneous Petrology,* p. 504, Freeman, San Francisco.

McKenzie, D.P., 1984. The generation and compaction of partially molten rock, *J. Petrol.,* **25,** 713–765.

Marsh, D.B., 1981. On the crystallinity, probability of occurrance, and rheology of lava and magma, *Contrib. Min. Pet.,* **78,** 85–98.

Marsh, D.B., 1988. Crystal capture, sorting and retention in convecting magma, *Geol. Soc. Am. Bull.,* **100,** 1720–1737.

Marsh, D.B., 1996. Solidification fronts and magmatic evolution, *Min. Mag.,* **60,** 5–40.

Martin, D., 1990. Crystal settling and *in-situ* crystallisation in aqueous solutions and magma chambers, *Earth. planet Sci. Lett.,* **96,** 336–348.

Mead, W.J., 1925. The geological role of dilatancy, *J. Geol.,* **33,** 685–698.

Molenkamp, F., 1985. Comparison of frictional material models with respect to shear band initiation, *Géotechnique,* **35,** 127–143.

Nicolas, A.A., 1986. A melt extraction model based on structural studies in mantle peridotites, *J. Petrol.,* **27,** 999–1022.

Paterson, M.S., 1995. A theory of granular flow accommodated by material transfer via an intergranular fluid, *Tectonophysics,* **245,** 135–151.

Paterson, S.R., Fowler, T.K., Schmidt, K.L., Yoshinobu, A.S., Yuan, E.S. & Miller, R.B., 1998. Interpreting magmatic fabric patterns in plutons, *Lithos,* **44,** 53–82.

Petford, N., 1993. Porous media flow in granitic magmas: an assessment, in *Flow and Creep in the Solar System: Observations, Modeling and Theory,* pp. 261–286, eds Stone, D.B. & Runcorn, S.K., NATO ASI 391.

Petford, N., 2003. Rheology of granitic magmas during ascent and emplacement, *Ann Rev. Earth. Planet Sci.,* **31,** 339–427.

Petford, N. & Koenders, M.A., 2001. Consolidation phenomena in sheared granitic magma: effects of grainsize and tortuosity, *Phys. Chem. Earth,* **26,** 281–286.

Renner, J., Evans, B. & Hirth, G., 2000. On the rheologically critical melt fraction, *Earth. planet. Sci. Lett.,* **181,** 585–594.

Reynolds, O., 1885. On the dilatancy of media composed of rigid particles in contact. With experimental illustration, *Phil. Mag.,* **20,** 469–481.

Rosenberg, C.L. & Handy, M.R., 2003. On the rheology of crustal rocks containing low melt fractions, *Geophys. Res. Abstracts,* **5,** 14 182.

Rowe, P.W., 1962. The stress dilatancy relation for static equilibrium of an assembly of particles in contact, *Proc. R. Soc. A,* **269,** 500–527.

Rutter, E.H. & Neumann, D.H.K., 1995. Experimental deformation of partially molten Westerly granite under fluid-absent conditions, with implications for the extraction of granitic magmas, *J. geophys. Res.,* **100,** 15 697–15 715.

Scott, D.R. & Stevenson, D.J., 1986. Magma ascent by porous flow, *J. geophys. Res.,* **91,** 9283–9296.

Sleep, N.H., 1988. Tapping of melt by veins and dikes, *J. geophys. Res.,* **93,** 10 255–10 272.

Spencer, A.J.M., 1964. A theory of the kinematics of ideal soils under plane strain conditions, *J. Mech. Phys. Solids,* **12,** 337–351.

Spiegelman, M., 1993. Flow in deformable porous media. Part 1 Simple analysis, *J. Fluid. Mech.,* **247,** 17–38.

Spiegelman, M., Kelemen, P.B. & Aharonov, E., 2001. Causes and consequences of flow organisation during melt transport, *J. geophys. Res.,* **106,** 2061–2077.

Stefanovska, E., 1996. Numerical simulation of an assembly of particles in elasto-frictional contact, *PhD thesis,* Kingston University.

Stevenson, D.J., 1989. Spontaneous small scale melt segregation in partial melts undergoing deformation, *Geophys. Res. Lett.,* **16,** 1067–1070.

Tait, S.R. & Jaupart, C., 1992. Compositional convection in a reactive crystalline mush and melt differentiation, *J. geophys. Res.,* **97,** 6735–6756.

Terzaghi, K., 1925. *Erdbaumechanik auf Bodenphysikalischer Grundlage,* Deuticke, Leipzig, p. 399.

Turner, J.S. & Campbell, I.H., 1986. Convection and mixing in magma chambers, *Earth Sci. Rev.,* **23,** 255–352.

Van der Molen, I. & Paterson, M.S., 1979. Experimental deformation of partially melted granite, *Contrib. Min. Pet.,* **70,** 299–318.

Vasilyev, O.V., Podladchikov, Y.Y. & Yuen, D., 1998. Modeling of compaction driven flow in poro-viscoelastic medium using adaptive wavelet collection method, *Geophys. Res. Lett.,* **25,** 3239–3242.

Vermeer, P.A., 1990. The orientation of shear bands in biaxial tests, *Géotechnique,* **40,** 223–236.

Vigneresse, J.L. & Tikoff, B., 1999. Strain partitioning during partial melting and crystallising felsic magmas. *Tectonophysics,* **312,** 117–132.

Vigneresse, J.L., Barbey, P. & Cuney, M., 1996. Rheological transitions during partial melting and crystallisation with application to felsic magma segregation and transfer, *J. Petrol.,* **37,** 1579–1600.

Wickham, S., 1987. The segregation and emplacement of granitic magmas, *J. geol. Soc. Lond.,* **144,** 281–297.

Worster, M.G., Huppert, H.E. & Sparks, R.S.J., 1990. Convection and crystallisation in magma cooled from above, *Earth. planet. Sci. Lett.,* **101,** 78–89.

APPENDIX: SOLUTION OF THE ONE-LAYER PROBLEM

The total excess stress $\boldsymbol{\sigma}$ is composed of the excess skeletal stress $\boldsymbol{\sigma}'$ and the fluid excess pore pressure p according to Terzaghi (1925): $\sigma_{ij} = \sigma'_{ij} - p\delta_{ij}$. The skeletal stress rate is linked to the strain rate $\dot{\mathbf{e}}$ and satisfies the constititutive law $\dot{\sigma}'_{ij} = a_{ijkl}\dot{e}_{kl}$. The vertical coordinate is called y, the horizontal one x. In the one-layer problem, pure shear is assumed to be applied and the problem is independent of x. This leaves the following constitutive relations:

$$\dot{\sigma}'_{11} = \frac{1}{2}a_{1112}\frac{\partial \dot{u}}{\partial y} + a_{1122}\frac{\partial \dot{v}}{\partial y}$$

$$\dot{\sigma}'_{12} = \frac{1}{2}a_{1212}\frac{\partial \dot{u}}{\partial y} + a_{1222}\frac{\partial \dot{v}}{\partial y}$$

$$\dot{\sigma}'_{21} = \frac{1}{2}a_{2112}\frac{\partial \dot{u}}{\partial y} + a_{2122}\frac{\partial \dot{v}}{\partial y}$$

$$\dot{\sigma}'_{22} = \frac{1}{2}a_{2212}\frac{\partial \dot{u}}{\partial y} + a_{2222}\frac{\partial \dot{v}}{\partial y},$$

where the displacement components are (u, v). Stress equilibrium and stress symmetry leave two relations with time-dependent constants $c(t)$ and $d(t)$,

$$\frac{\partial \dot{\sigma}'_{12}}{\partial y} = 0 \rightarrow \dot{\sigma}'_{12} = \dot{c}(t)$$

$$\frac{\partial \dot{\sigma}'_{22}}{\partial y} - \frac{\partial \dot{p}}{\partial y} = 0 \rightarrow \dot{\sigma}'_{22} - \dot{p} = \dot{d}(t).$$

The constant $d(t)$ represents the total vertical excess stress. The focus here is on processes where pure shear is applied in the absence of a simultaneously applied vertical stress and therefore $\dot{d}(t) = 0$.

Biot's equation expresses continuity of the fluid, compressible phase in a granular environment, assuming Darcyan porous medium flow with position-dependent permeability $k(\mathbf{x})$, see Biot (1941). It is specialized to the geometry to hand. If the porosity of the medium is n and the fluid compressibility is β' it reads

$$\frac{\partial}{\partial y}\left[k(y)\frac{\partial p}{\partial y}\right] = n\beta'\frac{\partial p}{\partial t} + \frac{\partial \dot{v}}{\partial y}.$$

The displacement gradient rates can be eliminated from the problem to give

$$\frac{\partial \dot{v}}{\partial y} = \frac{a_{1212}\dot{p} - a_{2212}\dot{c}(t)}{a_{1212}a_{2222} - a_{2212}a_{1222}}.$$

The signs of the moduli can now be read. In the absence of an isotropic stress rate an increasing shear stress will result in an increasing volumetric rate. The sign of $a_{2212}/(a_{1212}a_{2222} - a_{2212}a_{1222})$ must therefore be opposite to the sign of the shear stress increase. In practice this implies that a_{2212} must be negative, as the determinant can never be zero and in its evolution must have started from an isotropic state as a positive quantity $a_{1212}a_{2222}$.

Substituting the rate of volume strain in Biot's equation yields

$$\frac{\partial}{\partial y}\left[k(y)\frac{\partial p}{\partial y}\right] = n\beta'\dot{p} + \frac{a_{1212}\dot{p} - a_{2212}\dot{c}(t)}{a_{1212}a_{2222} - a_{2212}a_{1222}}.$$

This equation has general validity, but it is noted that the components of the incremental stiffness tensor $\boldsymbol{a}$ depend, generally speaking, on position and time.

In the geometry envisaged, the top of the region is at $y = 0$, the bottom is at $y = -H$ (see Fig. 2). The bottom is all fluid, implying that all components of $\boldsymbol{a}$ vanish and the permeability is infinite. Thus no excess pore pressure or skeletal stress exists in the vicinity of $y = -H$ and therefore (again) it is concluded that $d(t) = 0$. The top of the region is virtually impermeable and thus the pressure gradient must vanish here: $\partial p/\partial y = 0$.

Taking both $\boldsymbol{a}$ and k constants in the region $0 < y < -H$ Biot's equation is now solved. Recast it in the form

$$k\frac{\partial^2 p}{\partial y^2} = \left(n\beta' + \frac{a_{1212}}{a_{1212}a_{2222} - a_{2212}a_{1222}}\right) \times \dot{p} - \frac{a_{2212}\dot{c}(t)}{a_{1212}a_{2222} - a_{2212}a_{1222}}.$$

Introducing the auxiliary variables $\theta \equiv (a_{1212}a_{2222} - a_{2212}a_{1222})/a_{1212}$ and $R \equiv a_{2212}/[a_{1212}(n\beta'\theta + 1)]$, the equation is then Laplace transformed. The transformed parameters are denoted by a hat and the Laplace frequency is called λ,

$$\theta k\frac{\partial^2 \widehat{p}}{\partial y^2} = \left(n\beta'\theta + 1\right)\lambda\widehat{p} - R\left(n\beta'\theta + 1\right)\lambda\widehat{c}.$$

Now, defining $\mu \equiv \sqrt{(n\beta'\theta + 1)\lambda/(\theta k)}$,

$$\widehat{p}(y) = R\widehat{c}\left[1 - \frac{\cosh(\mu y)}{\cosh(\mu H)}\right] = R\widehat{c} - R\widehat{c}[\mathrm{e}^{\mu(y-H)} + \mathrm{e}^{-\mu(y+H)}]\sum_{m=0}^{\infty}(-1)^m\mathrm{e}^{-2\mu Hm}.$$

The inverse transform is found when the loading function is specified. Assume that the shear stress increases linearly with time: $c(t) = c_0 t$, with a constant rate $\dot{c}_0$, implying that $\widehat{c}(\lambda) = \dot{c}_0\lambda^{-2}$. One finds

$$p(y,t) = R\dot{c}_0 t - R\dot{c}_0\sum_{m=0}^{\infty}(-1)^m \times \left\{\frac{1}{2}\left[\left(a_m^2 + 2t\right)\mathrm{erfc}\left(\frac{a_m}{2\sqrt{t}}\right)\right] - \frac{a_m\sqrt{t}}{\sqrt{\pi}}\mathrm{e}^{-a_m^2/4t}\right\} - R\dot{c}_0\sum_{m=0}^{\infty}(-1)^m \times \left\{\frac{1}{2}\left[\left(b_m^2 + 2t\right)\mathrm{erfc}\left(\frac{b_m}{2\sqrt{t}}\right)\right] - \frac{b_m\sqrt{t}}{\sqrt{\pi}}\mathrm{e}^{-b_m^2/4t}\right\},$$

where $a_m = \sqrt{\frac{n\beta'\theta+1}{\theta k}}(H - y + 2Hm)$ and $b_m = \sqrt{\frac{n\beta'\theta+1}{\theta k}}(H + y + 2Hm)$.

Solutions for short and long times are easily obtained:

$$t \to 0 : p(y,t) = R\dot{c}_0 \left[t - \left\{ \frac{1}{2} \left[\left(a_0^2 + 2t\right) \operatorname{erfc}\left(\frac{a_0}{2\sqrt{t}}\right) \right] - \frac{a_0\sqrt{t}}{\sqrt{\pi}} \mathrm{e}^{-a_0^2/4t} \right\} \right],$$

where $a_0 = \sqrt{\frac{n\beta'\theta+1}{\theta k}}(H-y)$

$$t \to \infty : R\dot{c}_0 \frac{H^2 - y^2}{2k\theta}.$$

A natural scaling is present. All length-scales can be represented as fractions of H: $y = y^* H$; and all timescales as fractions of $H^2(n\beta'\theta + 1)/(\theta k)$: $t = t^* H^2(n\beta'\theta + 1)/(\theta k)$. The excess pore pressure furthermore scales as $p = p^* R\dot{c}_0 H^2/(\theta k)$ and the auxiliary variables a_m and b_m as $a_m^* H\sqrt{(n\beta'\theta + 1)/(\theta k)}$ and $b_m^* H\sqrt{(n\beta'\theta + 1)/(\theta k)}$. The solution for the excess pore pressure is now written as

$$p^*(y^*, t^*) = t^* - \sum_{m=0}^{\infty}(-1)^m \times \left[\frac{1}{2} \left\{ \left[(a_m^*)^2 + 2t^*\right] \operatorname{erfc}\left(\frac{a_m^*}{2\sqrt{t^*}}\right) \right\} - \frac{a_m^*\sqrt{t^*}}{\sqrt{\pi}} \mathrm{e}^{-(a_m^*)^2/4t^*} \right] - \sum_{m=0}^{\infty}(-1)^m \times \left[\frac{1}{2} \left\{ \left[(b_m^*)^2 + 2t^*\right] \operatorname{erfc}\left(\frac{b_m^*}{2\sqrt{t^*}}\right) \right\} - \frac{b_m^*\sqrt{t^*}}{\sqrt{\pi}} \mathrm{e}^{-(b_m^*)^2/4t^*} \right].$$